

Efficient treatment of rubber friction problems in industrial applications

K. Hofstetter[†], J. Eberhardsteiner[‡] and H. A. Mang^{‡†}

Institute for Mechanics of Materials and Structures, Vienna University of Technology, Vienna, Austria

(Received June 21, 2005, Accepted October 18, 2005)

Abstract. Friction problems involving rubber components are frequently encountered in industrial applications. Their treatment within the framework of numerical simulations by means of the Finite Element Method (FEM) is the main issue of this paper. Special emphasis is placed on the choice of a suitable material model and the formulation of a contact model specially designed for the particular characteristics of rubber friction. A coupled thermomechanical approach allows for consideration of the influence of temperature on the frictional behavior. The developed tools are implemented in the commercial FE code ABAQUS. They are validated taking the sliding motion of a rubber tread block as example. Such simulations are frequently encountered in tire design and development. The simulations are carried out with different formulations for the material and the frictional behavior. Comparison of the obtained results with experimental observations enables to judge the suitability of the applied formulations on a structural scale.

Keywords: friction; rubber; thermo-mechanical coupling; finite elements; tires.

1. Introduction

Coupled thermo-mechanical frictional contact problems involving rubber components are common to many industrial applications, e.g., tires, sealings, and wiper blades. Rubber is a high-molecular material. Because of its strongly viscous behavior and the rather low elastic modulus, rubber friction differs from the frictional behavior of most other solids. The following investigations are limited to vulcanized, particle-filled rubber, which is commonly used for engineering purposes.

This paper focuses on the simulation of rubber friction events by means of the Finite Element Method (FEM). The material behavior of rubber and (rubber) friction have received a lot of scientific interest (Wriggers 2002, Persson 2000, Klüppel and Heinrich 2000, Ogden 2001, Dorfmann and Ogden 2004, Dorfmann and Muhr 1999). However, there is often a gap between theoretical developments and practical applications at a structural scale. To fill this gap in the framework of rubber friction problems by suitable preparation of (existing) theoretical formulations is the main concern of this paper. For product design and development, the use of numerical analysis techniques has become a quite convenient and powerful tool. It helps to keep down

[†] Doctor, Corresponding author, E-mail: karin.hofstetter@tuwien.ac.at

[‡] Professor, E-mail: josef.eberhardsteiner@tuwien.ac.at

^{‡†} Professor, E-mail: herbert.mang@tuwien.ac.at

development costs and times. The performance of realistic numerical simulations implies the following main tasks:

- choice of a suitable material model for rubber which is capable of a realistic description of the involved strain states evolving in the considered simulations,
- establishment of a thermo-mechanically coupled contact model for rubber,
- implementation of the derived formulations in a FE code, appropriate specification of element formulations and algorithmic parameters for the simulations, and
- verification of the numerical results by means of experiments.

The intended suitability of the established simulation procedures for product development in industrial use brings about several demands. The established formulations must be simple and easily adaptable to be applicable for various purposes. Their implementation in commercial software packages has to be inexpensive. The resulting simulation procedures must work efficiently and reliably.

Engineering applications are generally concerned with the overall behavior of structural components. For example, tire engineers aim at maximization of the tangential force transferred from the tire to the road. Consideration of local phenomena is limited to a correct representation of their influence on the overall structural behavior. This motivates a macroscopic approach for the numerical simulations, which is also favorable with regard to industrializability. Neither the molecular structure of rubber nor the roughness of the contact surfaces are taken into account in an explicit manner. As regards the contact zone, perfectly smooth surfaces are assumed. Contact interactions are modeled in terms of shear stresses and heat fluxes at the contact interface, resulting from local deformations of the rubber block at the asperities of the rough contact surface and associated heat generation and heat conduction. Only the resulting remarkable reduction of effort for discretization allows for the use of the contact model in technical applications. Consideration of surface asperities in the FE model, as required in a microscopic approach, is not feasible in this case. The effect of surface roughness is included in the formulations for the contact model by means of statistical parameters of the surface profile.

The establishment of a suitable simulation procedure is demonstrated taking the sliding motion of a rubber tread block as example. Such simulations are used in tire industry at an early stage of tire development. The sliding of a tread block resembles the processes in the contact zone of a tire in ABS braking events as indicated in Fig. 1. During ABS braking, the tire remains in a rolling

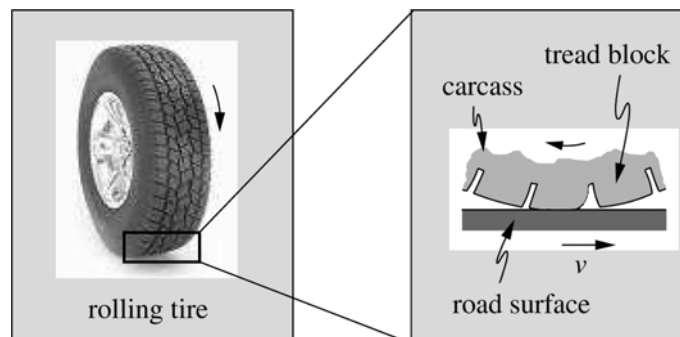


Fig. 1 Contact between tire and road

motion. Its tread blocks subsequently make up contact with the road surface, slide a short distance according to the slip inherent to the ABS system, and then detach again. Consequently, each tread block faces a succession of short sliding periods in between of longer unloaded periods, during which the tire accomplishes a revolution. A single tread block is a simple structure compared to complete tread patterns or whole tires. In the simulations, this simplicity enables the separation of material effects from structural effects, which occur when rubber blocks are arranged in real tread patterns.

Different formulations for the material as well as the contact behavior are introduced and applied in the addressed simulations. Their influence on the structural behavior of the blocks and, in turn, on the quality of the simulation results is critically assessed. Experimental investigations of sliding tread blocks serve as reference basis for the validation.

The paper is organized in four main parts. The first part deals with the material model. Possible mathematical formulations are presented. Furthermore, experimental investigations and parameter identification procedures in this context are outlined. The second part focuses on the contact model. It makes up the main part of the paper. Mechanical as well as thermal effects at the contact surface are examined and put into suitable formulations. The determination of involved parameters and accompanying tests are shortly discussed. The third part demonstrates the implementation of the established model in a commercial FE code. Its application for the numerical simulation of a rubber sliding process is shown by means of an introductory example. Finally, the fourth part is dedicated to a discussion of the simulation results, which make up the basis for validation of the established numerical model. Necessary improvements and further extensions are indicated. Conclusions drawn from the simulation results close the paper.

2. Material model

2.1 Mathematical formulation

The choice of a suitable constitutive model for rubber is of vital importance for the quality of the results of numerical simulations. The material behavior of rubber is very complex. Depending on temperature and velocity of excitation, the characteristics of rubber range from extremely brittle and glassy to compliant and even fluid-like. A comprehensive mechanical description requires elastic, viscous, and plastic elements in combination with a suitable formulation for the effects of material damage.

Under negligence of any inelastic effects, rubber can be classified as hyperelastic material. Its behavior is characterized by an unambiguous stress-strain relationship. No history dependence exists. Thus, a potential of the strains can be defined (the *strain energy*), which allows for computation of the stresses by differentiation of the potential with respect to the strains. Material models for rubber are usually formulated in terms of the strain energy. Since rubber exhibits a nearly incompressible material behavior, only deviatoric contributions to the strain energy function need to be regarded. Formulations for this function are mostly based on either theoretical considerations about the macromolecular microstructure of rubber or on experimental results obtained with macroscopic rubber samples. Microstructurally motivated formulations represent the underlying physics of the material behavior. This parameters are intrinsic characteristics of the materials. However, the formulations are generally rather sophisticated, and the involved parameters

difficult to identify. The use of macroscopic experimental data as basis for the derivation of a material model yields phenomenological formulations. A pile of such formulations exists (see, e.g., Kaliske and Rothert 1997 or Kaliske 1995 for a review). They differ in their degree of complexity and the number of involved material parameters. In general, all formulations suffer from the same deficiency of “non-physical” parameters. The consequence are a dependence of the parameters on the kind of experimental data used for their identification and a lack of predictive capability of such models.

Within the scope of this paper, three different formulations for the material behavior are used in the further examinations:

- The Mooney-Rivlin model is the standard material model for rubber in most engineering applications. The strain energy function proposed by this model reads:

$$U^{MR} = C_{10}^{MR}(\bar{I}_1 - 3) + C_{01}^{MR}(\bar{I}_2 - 3) \quad (1)$$

with two material parameters C_{10}^{MR} and C_{01}^{MR} . \bar{I}_1 and \bar{I}_2 denote the first and second invariant of the left Cauchy-Green strain tensor. The model involves solely first order terms and, consequently, can not represent the upturn (i.e., steep rise) of the stress-strain curve at high strain. This upturn results from the approach of the rubber deformation to the locking stretch, which marks the maximum extensibility of the polymer chains. Therefore, the Mooney-Rivlin model is only suitable for small and moderate strains. Besides the limited suitability in terms of strain range, the model shows remarkable deficiencies when applied for biaxial loading states. Remarkable deviations between computed and experimentally observable material behavior result, especially if only uniaxial test data are available for the identification of the material parameters. The addressed shortcomings of the Mooney-Rivlin model are well-known. Their consequences in view of technical applications are discussed in the framework of the presented simulations of tread blocks.

- The Yeoh model is – besides the Mooney-Rivlin model – another example of a phenomenological formulation. The strain energy function for this model reads

$$U^Y = C_{10}^Y(\bar{I}_1 - 3) + C_{20}^Y(\bar{I}_1 - 3)^2 + C_{30}^Y(\bar{I}_1 - 3)^3 \quad (2)$$

Three material parameters C_{10}^Y , C_{20}^Y and C_{30}^Y are involved this case. The model generally allows for a rather good fit of experimental results, although it still uses a quite simple formulation. The dependence on the second strain invariant is omitted, while higher order terms of the first strain invariant are included.

- The van der Waals model is a representative of the class of physically motivated formulations. Compared to most other models on polymer-statistical basis, it is rather simple. It is probably the best-known and most widely applied material model for rubber with a microstructural foundation. A constitutive equation of the type generally employed for ideal gases is used for the polymer network. The involved material characteristics are the initial shear modulus μ_0^W , the locking stretch λ_m , and a global interaction parameter a . The strain energy function U^W on basis of these parameters reads

$$U^W = \mu_0^W \left\{ -(\lambda_m^2 - 3)[\ln(1 - \eta) + \eta] - \frac{2a}{3} \left(\frac{\tilde{I} - 3}{2} \right)^{\frac{3}{2}} \right\} \quad (3)$$

where

$$\tilde{I} = (1 - \beta)\bar{I}_1 + \beta\bar{I}_2 \quad \text{and} \quad \eta = \sqrt{\frac{\tilde{I} - 3}{\lambda_m^2 - 3}} \quad (4)$$

The parameter β represents a linear mixture parameter that combines the influence of the invariants \bar{I}_1 and \bar{I}_2 . It is set to zero in the following investigations.

Extension of the material model to consideration of viscous effects and damage may be necessary depending on the characteristics of the specific application. In this paper, main focus is on frictional sliding of rubber tread blocks. The sliding events are generally characterized by short duration and the limitation of high-frequent load changes to the immediate vicinity of the contact surface. This allows for disregard of time-dependent effects for the bulk material, provided that local effects in the contact zone are captured in the (macroscopic) contact conditions.

Similar arguments apply to the effect of material damage, whereas attention must be paid to exclude the influence of the Mullins effect by an appropriate choice of experimental data for the parameter identification, as indicated below.

In general, not only the choice of appropriate formulations for the material description is essential, but also the use of suitable and sufficiently comprehensive data for the parameter identification. The testing mode exerts an influence on the obtained parameters as well as the velocity of loading and the amplitude of straining. Because of material damage, the prestrain of the rubber samples affects the results. Furthermore, loading and unloading curves generally do not coincide. The experiments which served as basis for the parameter identification in the work at hand are described in the next Subsection. The extraction of a suitable dataset from these experiments for the identification procedure is sketched as well.

2.2 Experimental investigations and parameter identification

In the presented investigations, parameter identification is based on experimental data from uniaxial tests with dumbbell-shaped and bar-shaped test specimens. The compact dumbbell shape allows for examination of the material behavior not only in tension, but also in compression. The diameter of the dumbbells amounts to approximately 20 mm. The test procedure is such that the strain is gradually increased for each specimen in steps of 10% in the tension range, alternating with steps of about 5% in the compression range. Several load cycles are run at each strain level. A detailed description of the test procedure can be found in Hofstetter (2004).

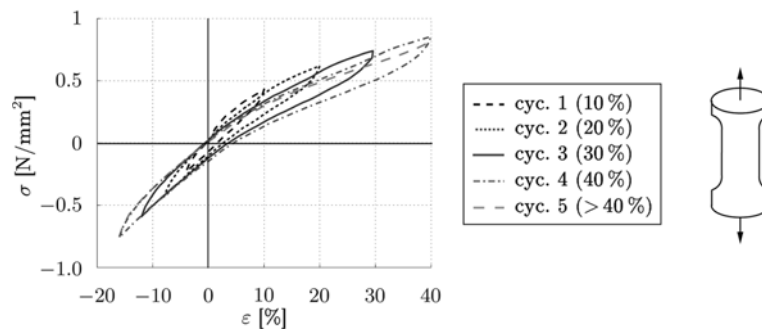


Fig. 2 Experimental stress-strain curves for dumbbell-shaped test specimens

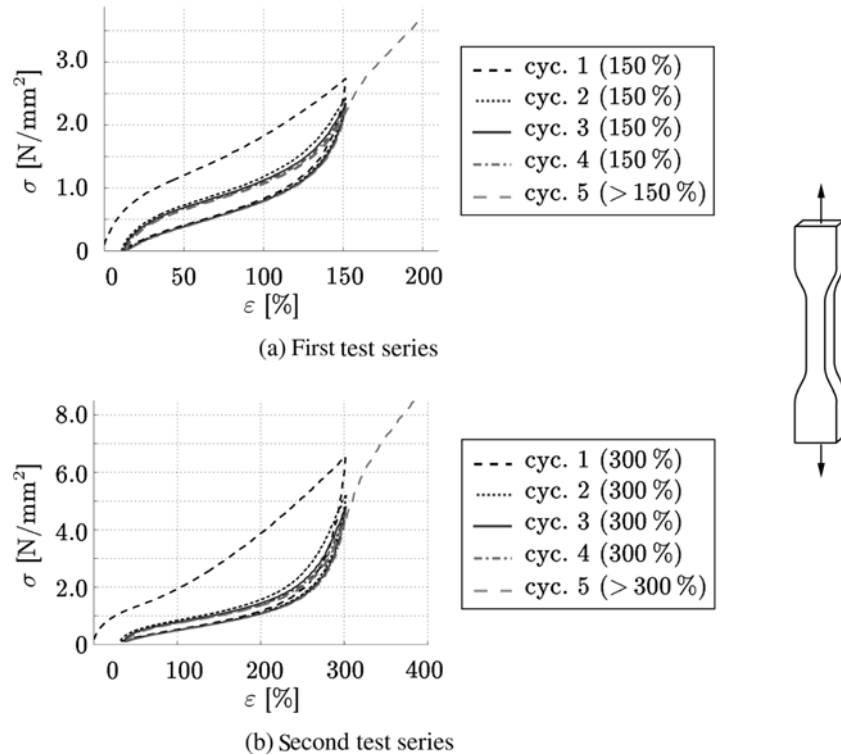


Fig. 3 Experimental stress-strain curves for bar test specimens

The results are shown in Fig. 2, in which only the first cycle at each strain level is plotted. The denotation “cyc. 5” refers to the last loading in the test, where the dumbbells are stretched until failure. The shortcoming of these tests is that only a very narrow range of strains from approximately -18% to 40% is covered.

With the bar-shaped test specimens, two test series were performed. They differed in the investigated strain range, but were run under identical conditions otherwise. The maximum strain amplitude amounted to 150% in the first and to 300% in the second series. Compared to the dumbbell tests, a much more extensive strain range in the tension domain was examined in these tests. However, investigation of the compression domain is not possible with the bars. Their slenderness would cause buckling already at very small strain levels. Every bar is stretched five times up to the maximum strain amplitude, before it is loaded once more until failure. The lower turning point is fixed at zero load. The tests are carried out at room temperature with a strain velocity $v = 400$ mm/min. Further details about the test procedure with bar-shaped test specimens are given in Hofstetter (2004). The resulting stress-strain curves are depicted in Fig. 3.

In order to cut down the influence of material damage on the test results as far as possible, data from the last full load cycle – i.e., the last entire load cycle that includes loading as well as unloading – at the highest strain level is evaluated. This cycle generally corresponds to a more or less stable material behavior. In relation to different material formulations and material tests, several parameter sets are identified for an exemplary rubber compound. A collection of the resulting sets

Table 1 Sets of material parameters for an exemplary rubber compound and different material models

	C_{10}^{MR} [N/mm ²]	C_{01}^{MR} [N/mm ²]	
Mooney-Rivlin, dumbbells	0.2580	0.4587	
	C_{10}^Y [N/mm ²]	C_{20}^Y [N/mm ²]	C_{30}^Y [N/mm ²]
Yeoh, bars, series 1	0.3494	-0.05272	0.01295
Yeoh, bars, series 2	0.3200	-0.02000	0.00190
Yeoh, bars, series 1, load	0.3794	0.02320	-0.00030
	μ_0^W [N/mm ²]	λ_m [-]	a [-]
van der Waals, bars, series 1	0.7500	3.5000	1.0000
van der Waals, bars, series 2	0.6000	4.9500	0.6800

of material parameters is provided in Table 1. The parameters for the Mooney-Rivlin model are determined with data exclusively from dumbbell tests. Data from tests with bars reach into the upturn region, which is not reproducible by this material model. Unsuitable material parameters would be obtained with these data. The material parameters for the Yeoh and for the van der Waals model, on the contrary, are determined with data from bar tests only. Two parameter sets are identified based on one of the two test series with bars each. The dumbbell tests do not cover any information about the upturn of the stress-strain curve and, consequently, do not provide sufficient input data for these models. An additional parameter set was identified for the Yeoh model (denotation “load”, Table 1) for comparison purposes. Contrary to the general practice of using loading and unloading data, only data from the loading path was employed for the identification of this set.

3. Contact model

3.1 General considerations

The contact model provides a description for mechanical and thermal interactions at the contact surface. The derivation of suitable analytical formulations requires a profound knowledge of the characteristics of rubber friction and its physical basics on the microscale. At this scale, the contact surfaces are not perfectly smooth. The surface roughness limits the contact area to a few contact spots developing at the highest surface asperities. Rubber friction is hysteretic friction for the most part. Because of the roughness of the contact surface periodic deformations of the rubber layers adjacent to the contact interface occur at every pass of a contact spot. The internal energy cannot be fully restored, as the deformations recede, in consequence of the viscous behavior of rubber. At a macroscopic scale, this energy dissipation appears as a force opposing the direction of sliding. This force is denoted as hysteretic friction force. The main share of the dissipated energy is converted into heat. It results in a temperature increase at the contact surface and in regions of the rubber block adjacent to this surface. Heat fluxes in the bulk of the involved solids as well as across the contact surface are brought about.

Recently, models for the derivation of contact formulations on a microscale are increasing in popularity. A microscopic approach considers the composition of the contact surfaces of single asperities. It allows for the investigation of the underlying physical mechanisms of contact. The final macroscopic formulations are commonly obtained by homogenization. In the homogenization step, the interactions between the single microscale asperities are smeared to result in macroscopic relations for the description of the contact behavior. Thereby, mechanical contact interactions at a microscale can be examined numerically (e.g., by means of the FEM) (Haraldsson and Wriggers 2000, Twardzydlo *et al.* 1998, Chantrenne and Raynaud 2001) or analytically (Persson 2000, Klüppel and Heinrich 2000, Majumdar and Tien 1991).

Besides microscale models, formulations for the contact behavior can be obtained on a phenomenological basis. Experimental observations are used for the determination of the influence of surface roughness, rubber compound, and other contact parameters on the contact behavior in this case. The approach presented in this paper pursues the latter strategy. Its main advantage compared to the use of micromodels is the substantial reduction of complexity and expense without corresponding loss in affinity to reality. The contact formulations obtained with this approach are described in the next two subsections. Mechanical and thermal aspects are treated separately.

3.2 Mechanical interactions at the contact interface

Mechanical interactions at the contact interface include transfer of tangential shear stresses and normal stresses between the contact partners. This transfer actually takes place at the contact spots, which are not resolved in a macroscopic approach. A continuous stress distribution is assumed for this reason, which is obtained by smearing of the discrete stress concentrations. The smeared shear stress is computed as product of the local contact pressure p and a friction coefficient μ . Experimental investigations show that the friction coefficient is affected by many characteristics of the particular contact situation. The main effects emanate from the contact pressure p and the sliding velocity $v = \|\mathbf{v}\|$. Two different formulations for the friction coefficient, depending on these parameters, are considered: a comparably simple exponential relation and a more sophisticated formulation proposed by Huemer *et al.* (2001). The formulations for the friction coefficient with p and v as independent variables will be denoted as *friction laws* in the following.

A straightforward formulation for a friction law is an exponential relationship in the form

$$\mu = A|p|^B\|\mathbf{v}\|^C \quad (5)$$

It is a purely phenomenological formulation without a physical or micromechanical foundation. The three parameters A , B and C allow for an adaptation of the friction coefficient to properties of the friction surface and the materials of the contact partners. They are identified by means of experimental investigations (cf. Subsection 3.4).

The friction law by Huemer reads as

$$\mu(p, \mathbf{v}) = \frac{\alpha|p|^{n-1} + \beta}{a + \frac{b}{\|\mathbf{v}\|^{1/m}} + \frac{c}{\|\mathbf{v}\|^{2/m}}} \quad (6)$$

It contains seven parameters α , β , a , b , c , n , and $1/m$, enabling a fit of the formulation to experimental results. Fig. 4 illustrates the course of μ as function of p and v for an exemplary set of

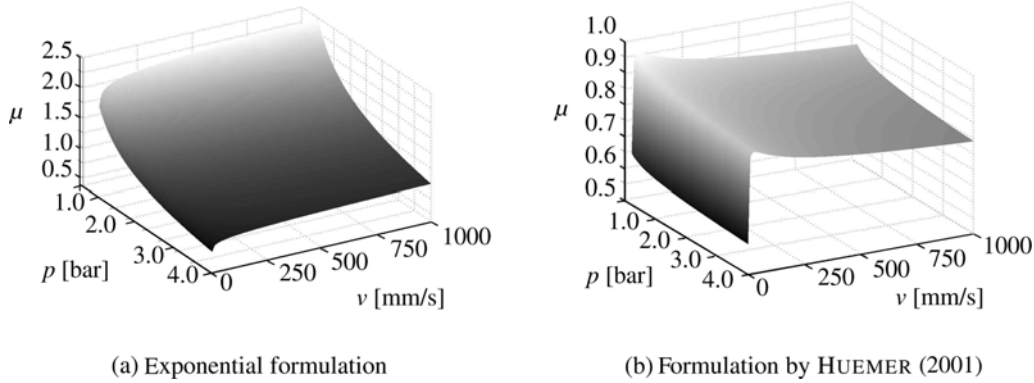


Fig. 4 Friction coefficient μ as function of sliding velocity \mathbf{v} and contact pressure p

parameters. Each subfigure refers to one formulation of the friction law.

In case of elevated temperatures of the rubber block, molecular motion is enhanced. The same effect can be observed in case of an increase of the excitation frequency and, consequently, an increase of the sliding velocity. Increases in temperature and in frequency obviously have similar influences on the viscoelastic properties of rubber. This also applies to the frictional behavior of rubber. The similarity allows for calculation of an equivalent sliding velocity in case of a temperature change instead of considering the temperature change explicitly. The necessary formulas for the determination of the equivalent sliding velocity were first published by Williams *et al.* (1955), motivating the denotation WLF-transformation. This transformation has become a well-accepted and generally used tool in dealing with polymers subjected to temperature changes. The equivalent sliding velocity follows from

$$\|\mathbf{v}_{equ}\| = \frac{a_{T,ref}}{a_{T,equ}} \|\mathbf{v}_{ref}\| \quad (7)$$

The coefficients $a_{T,ref}$ and $a_{T,equ}$ in (7) refer to the reference and the equivalent temperature, respectively. They are defined by

$$\log_{10} a_{T,s} = \frac{d_1(T - T_s)}{d_2 + (T - T_s)}, \quad s = \{ref, equ\} \quad (8)$$

d_1, d_2 denote material parameters. They are shift factors for the master curves, which represent the complex modulus as a function of frequency. A comprehensive description of the master curve technique can be found, e.g., in a monograph by Sperling (1992).

3.3 Thermal interactions at the contact interface

The frictional energy dissipation mainly results from periodic deformations of the rubber in layers adjacent to the contact surface. Hence, heat is not generated directly at the contact surface, but in the bulk of the material. The extension of the affected layer is very small compared to the overall dimensions of the rubber block. The spatial distribution of the heat sources is negligible in a macroscopic model for this reason. Concentrated heat sources at the bottom surface of the rubber block are assumed instead. The strength of these heat sources, q_{gen} , is defined as a partition of the

rate of energy dissipation, $\dot{E}_{diss} = \mathbf{v} \cdot \boldsymbol{\tau}_T$, reading as

$$q_{gen} = \kappa \dot{E}_{diss} = \kappa (\mathbf{v} \cdot \boldsymbol{\tau}_T) \quad (9)$$

In (9), \mathbf{v} denotes the (vectorial) sliding velocity, and $\boldsymbol{\tau}_T$ is the (vectorial) tangential shear stress at the contact surface. The partition coefficient κ accounts for the consumption of frictional energy by other energy modes than heat and for the loss of some heat to the subgrade. The establishment of a suitable formulation for κ is not easy. It is difficult, if not impossible, to access by either analytical, numerical, or experimental means. Its analytical or numerical assessment requires the formulation of an integrative energy balance. Inelastic deformations, material failure, and abrasion must be considered to cite just a few effects. Obviously, such a balance exceeds the capabilities of nearly all analytical models. The same arguments apply for a numerical approach.

The direct assessment of the amount of heat generation by experimental means is still more complicated and practically inapplicable. The heat delivery into the system was computable (though in very lengthy and complex calculations), if the temperature field in the rubber and the road surface was known at all time instances. However, the complete measurement of the temperature distribution in the entire contact pairing, which is fully three-dimensional, is not possible.

In this work, experimental measurements of the temperature distribution at the rubber contact surface are exploited for the specification of κ . Discrete estimates for selected magnitudes of the contact pressure p are determined by tuning of numerical simulations to match the corresponding experimental observations. An exponential relationship for κ with p as independent variable gives a good approximation of these estimates. The according fitting procedure is described in detail in Subsection 3.4.

In addition to fluxes q_{gen} from heat generation, also heat fluxes resulting from heat conduction at the contact interface have to be considered. Gap heat conduction occurs in case of different surface temperatures of the rubber block and the friction surface. The strength of the resulting heat flux, q_{con} , is determined as the product of the temperature difference ΔT and the heat transfer coefficient h :

$$q_{con} = \Delta T \cdot h \quad (10)$$

h strongly depends on the ratio of the nominal area of contact to the real one. Heat exchange between the two solids in contact occurs for the most part at the solid contact spots, which constitute the real contact area. Theoretically, heat is also transferred across the air-filled asperities between the contact spots by means of heat conduction and heat convection. However, this contribution to the total heat flux is negligibly small.

Thermal and mechanical characteristics of the contacting solids (e.g., conductivity and stiffness) as well as geometric properties of their surfaces (e.g., mean roughness) are the main parameters of the heat transfer coefficient. A relation proposed by Mikic *et al.* (1974) is taken as basis and is reformulated in order to meet the conditions of the contact problems at hand. Especially the elastic behavior of rubber even under high contact pressures must be regarded, which is not encountered for most other materials. Furthermore, the influence of excitation frequency and, thus, of sliding velocity on the material behavior of rubber must be taken into account. The following relation results for the heat transfer coefficient:

$$h = C \frac{\bar{k} |\bar{\zeta}_p|}{\tilde{\sigma}} \left(\frac{p\sqrt{2}}{\bar{E}(v) |\bar{\zeta}_p|} \right)^{0.94} \quad (11)$$

A detailed discussion of the derivation of (11) is provided in Hofstetter (2004). In (11), \bar{k} denotes the mean thermal conductivity of the two solids in contact, which is defined via its inverse as

$$\frac{1}{\bar{k}} = \frac{1}{2} \left(\frac{1}{k_1} + \frac{1}{k_2} \right) \quad (12)$$

k_1 and k_2 designate the thermal conductivity of rubber and subgrade. $\bar{E}(v)$ denotes the (velocity dependent) effective elastic modulus, reading as

$$\bar{E}(v) = \frac{E_1(v)E_2}{E_2(1 - \nu_1^2) + E_1(1 - \nu_2^2)} \quad (13)$$

where $E_1(v)$, ν_1 and E_2 , ν_2 are pairs of elastic modulus and Poisson ratio for rubber and subgrade, respectively. The elastic modulus of rubber, $E_1(v)$, is treated as velocity dependent quantity to account for the influence of velocity on the material behavior of rubber. The terms $\tilde{\sigma}$ and $|\bar{\zeta}_p|$ describe the mean gradient and the RMS roughness of the surface profile. They refer to the sum surface, which follows from a point-wise summation of the heights of both surface profiles. p is the local contact pressure. The constant C has to be determined by experiments (see Subsection 3.4).

3.4 Experimental investigations

The contact model involves a couple of parameters, which require experimental investigations for their identification. Most experiments are carried out at a testing device denoted as *Linear Friction Tester (LFT)* (Eberhardsteiner *et al.* 1998). This device is designed for the investigation of the sliding behavior of rubber tread blocks. It has been developed at the Laboratory of the Institute for Mechanics of Materials and Structures at Vienna University of Technology on behalf of Continental AG. The device pulls rubber blocks along straight lines over rough surfaces. These surfaces are cut out of real road surfaces in order to approach the conditions at real roads as closely as possible.

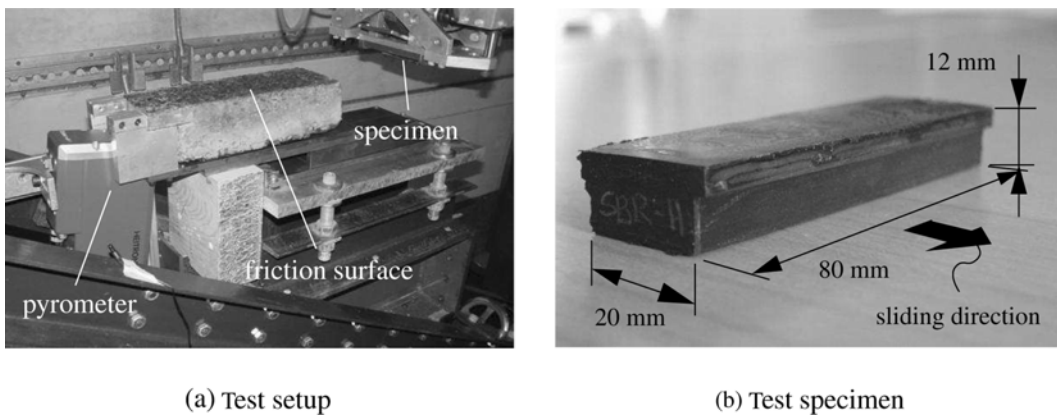


Fig. 5 Linear Friction Tester: photos of (a) the test setup and (b) a test specimen

Table 2 Parameters of the investigated formulations for the friction coefficient

(a) Exponential law		(b) Law by Huemer			
A	0.7064	α	0.1399	a	0.9203
B	-0.0645	β	0.4091	b	-1.1188
C	0.0425	n	0.8680	c	0.9677
		$1 = m$	0.1672		

Fig. 5 shows photos of the testing device and of the rubber test specimen with the simplest geometry. The main components of the test device and the overall dimensions of the specimen are specified in the photos.

The experiments are usually carried out in two consecutive steps. In the first step, uniform pressure is applied to the rubber block in a fixed position. Afterwards, the block is moved in sliding direction, while the pressure is maintained. The sliding velocity is held at a constant value during the whole experiment with exception of short periods of acceleration and deceleration at the beginning and the end of the motion.

During the experiment, horizontal and vertical forces acting on the rubber block are recorded. Their relation yields an integral friction coefficient. The temperature distribution at the bottom surface of the rubber block is measured by means of a radiation pyrometer installed at the end of the friction surface. Furthermore, the deformation behavior is observed in a qualitative manner by means of a highspeed digital camera. Besides the type of friction surface and the geometry of the rubber block, rubber compound, environmental temperature, sliding velocity, and contact pressure are the main parameters of the experiments.

The integral friction coefficients are employed for the identification of the parameters of the friction laws according to (5) and (6). The parameters for an asphalt contact surface and a rubber compound for use in winter tire treads, are compiled in Table 2.

Within the scope of the thermal contact model, the parameters κ for the heat generation and C for the heat conduction have to be determined. Similar strategies are pursued in both cases. Experimental investigations comprising temperature measurements are resimulated by means of the FEM in a thermo-mechanical manner. The formulations (9) and (11) are used for the definition of heat generation and conduction in the simulations using different settings of the parameters κ and C . Temperatures evaluated either at the contact surface or in the interior of the rubber block serve as verification criteria. Their measured and computed values are compared and allow for a tuning of the numerical simulations. The simulation with the best match of computed and measured temperatures yields an estimate for the parameters of the thermal contact model.

The parameter C in the formulation for the thermal contact conduction h , according to (11), is identified first. The temperature field in the entire rubber block and in parts of the road surface is assessed for this purpose. Since the thermal actions in the contact surface of a sliding block are difficult to examine, a purely static investigation is performed. Thereby, the heat transfer between a rubber block and a subjacent road surface in case of heating of the rubber block from its top is determined. The main components of the test setup are a rubber test specimen without sipes, a copper block, a heating element, and the asphalt friction surface used at the LFT. As obvious from Fig. 6, the heating element is placed on the top of the copper box, which in turn is situated at the top surface of the rubber block. The copper box serves as heat distributor to ensure a uniform heat input into the rubber test specimen. The unit composed of the rubber block, the copper box, and the

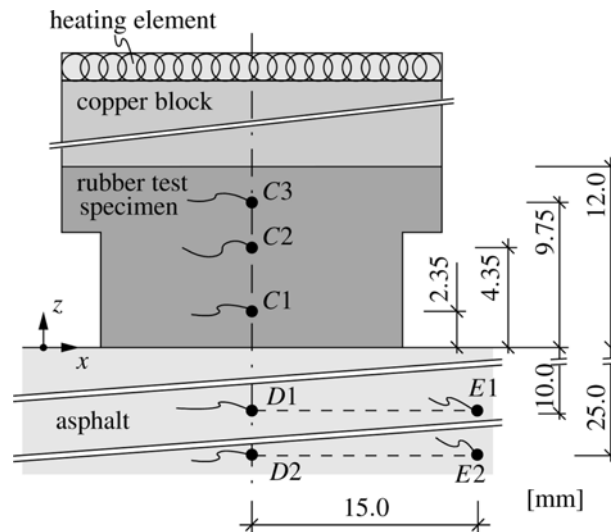


Fig. 6 Sketch of the experimental setup for the determination of the thermal contact conduction in stationary contact

heating element is placed on an asphalt block commonly used as friction surface at the LFT. It is fixed by means of clampings. They exert a nominal contact pressure of approximately 0.3 N/mm^2 , which is controlled by means of load cells.

The whole system is heated until stationary thermal conditions are attained. The temperature development in the rubber block and in the subjacent asphalt block is monitored during the heating and also during the cooling phase. Thermocouples integrated into the rubber specimen and the asphalt block are used for this purpose. Fig. 6 shows the positions of these thermocouples ($C1$, $C2$, $C3$, $D1$, $D2$, $E1$, and $E2$). Furthermore, the main dimensions of the experimental setup are specified there. The insertion of thermocouples in only the center line is sufficient, since the temperature field in the rubber block is approximately uni-directional. The large extensions of the asphalt block, compared to the dimensions of the area in contact with the rubber block, hinder the development of a uni-directional temperature field there. Thus, two more thermocouples ($E1$ and $E2$) are installed at a distance of approximately 15 mm from the center line.

Resimulation and comparison yields $h = 1600 \text{ W/(m}^2\text{K)}$ as optimal choice in case of a contact pressure $p = 0.3 \text{ N/mm}^2$. A detailed description of the resimulation procedure can be found in Hofstetter (2004). Having determined the magnitude of h , the parameter C in the formulation for h according to (11) follows straightforward. Eq. (11) is evaluated with the roughness and material properties of the experimental setup and the estimate for h from the resimulation.

For the determination of κ , the sliding motion at the LFT is resimulated. The default FE model, as described in Section 4, is used for this purpose. The temperature distribution at the contact surface after a certain sliding distance is measured by the pyrometer and compared with according simulation results. That way estimates for the partition coefficient for discrete settings of the sliding velocity and the contact pressure are obtained. The influence of the velocity on this coefficient turned out to be negligible. Thus, a formulation depending solely on contact pressure was chosen. An exponential relationship yields a good approximation for κ , reading as

$$\kappa = 0.3146p^{-0.6833} \quad (14)$$

The decreasing trend with pressure is in agreement with the underlying physical mechanisms. The higher the pressure, the larger the amount of abrasion, and the higher the probability of material failure and damage. Thus, the portion of the entire energy dissipation converted into heat reduces with increasing pressure.

4. Numerical simulations

4.1 FE model and implementation in ABAQUS

The thermo-mechanical simulations of the sliding behavior of rubber tread blocks are carried out by means of the commercial FE code ABAQUS (releases 6.2-5 and 6.3-1). Its version on basis of an explicit dynamic formulation (ABAQUS/Explicit) is used. An explicit code is chosen for reasons of efficiency and improved performance in contact problems. To check the suitability of the code for the simulations at hand, accompanying simulations with an implicit code were performed for selected problems. They revealed a good agreement of results obtained with the different codes.

All considered material models (the Mooney-Rivlin, the Yeoh, and the van der Waals model) are readily available in ABAQUS. Also with regard to the contact model, ABAQUS provides several predefined options. Interfaces to user subroutines are installed that allow for the definition of complex formulations for the friction coefficient and the thermal contact conduction. From an algorithmic viewpoint, ABAQUS/Explicit uses a kinematic contact algorithm of predictor-corrector type for the enforcement of contact.

The rubber test specimens have a large extension in the lateral direction, i.e., normal to the sliding direction, resulting in approximately plane strain state conditions in a middle cross-section of the rubber block. This motivates the use of 2D models in the numerical simulations. The suitability of these models for representation of the straining in the middle cross-section was confirmed by comparing FE-simulations with three-dimensional models (Hofstetter *et al.* 2005).

Fig. 7 shows the discretization of the cross-section of the rubber block. Elements with bilinear interpolation of displacements and temperature (type Q1/T1), reduced integration and hourglass stabilization on basis of an enhanced assumed strain concept are used for the discretization of the rubber block. A refinement of the mesh adjacent to the contact surface and at the leading edge is necessary to resolve the steep pressure and temperature gradients there. The thermo-mechanical input parameters of the rubber block are summarized in Table 3.

Table 3 Thermo-mechanical input parameters of rubber and asphalt

Characteristics	Units	Rubber	Asphalt
WLF-shift factor d_1	–	43.1	–
WLF-shift factor d_2	–	509.4	–
Mass density ρ	kg/m ³	1207	2000
Thermal conductivity λ	W/(m K)	0.284	0.70
Heat capacity c	kJ/(kg K)	1.45	0.92

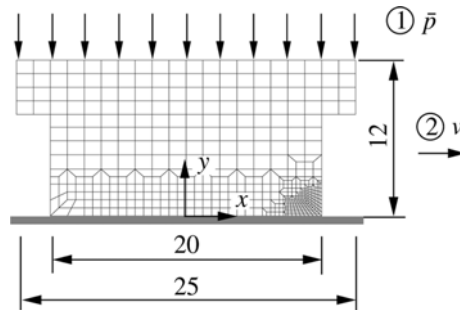


Fig. 7 Rubber block: cross-section, dimensions [in mm] and FE-mesh

During the simulation, parts of the bottom surface of the rubber block make up contact with each other. Contact between rubber surfaces is modeled by means of a Coulomb friction law with a (constant) friction coefficient of 1.0. The latter was determined by experiments at the LFT. It refers to a mean value of measured friction coefficients in different test runs. As regards thermal interactions, frictional heat generation is considered in rubber-to-rubber contact. No heat transfer by heat conduction is taken into account. Since the contacting rubber surfaces generally show comparable temperatures, this simplification is reasonable.

As regards thermal boundary conditions, all free surfaces are modeled as radiative surfaces with an emissivity of 0.9. Surfaces currently in contact are subject to thermal contact conditions as described in Subsection 3.3.

The road serving as friction surface is modeled as rigid. This idealization is admissible because of the large difference between the stiffnesses of rubber and asphalt, respectively. It considerably speeds up the simulations without provoking loss of accuracy. For the simulation of the thermal behavior, the road surface is discretized with elements of type T1 (linear interpolation of temperature). In the presented simulations, asphalt is chosen as material for the road. The required thermal input parameters are included in Table 3, too.

The FE-simulation is performed in two steps as illustrated in Fig. 7. In the first step ①, a uniformly distributed pressure \bar{p} is applied at the top of the rubber block. Under maintenance of this pressure, the block is moved at constant sliding velocity v in the second step ②.

4.2 Simulation results

The simulation of the sliding motion of a rubber block with $v = 300$ mm/s and $\bar{p} = 0.25$ N/mm² (which results in an average contact pressure $p = 0.3$ N/mm²) is investigated as introductory example. The Yeoh material model with parameters on basis of the first test series with bars and data from the loading path only is used (denotation “Yeoh, bars, series 1, load”, Table 1). For the definition of the friction behavior, the law by Huemer is applied. Fig. 8 shows the deformed mesh as well as the distributions of temperature T and normal stress in vertical direction, σ_y . The results are evaluated at a sliding distance $g_T = 120$ mm, where g_T is the displacement of a point at the top surface of the rubber block in sliding direction (along the x -axis).

Detailed views of the front edge are included in Fig. 8 in order to resolve the temperature and stress distributions there. Different scales are chosen for these representations and for the overall views of the entire block. At the leading edge, there is a concentration of contact pressure, so that

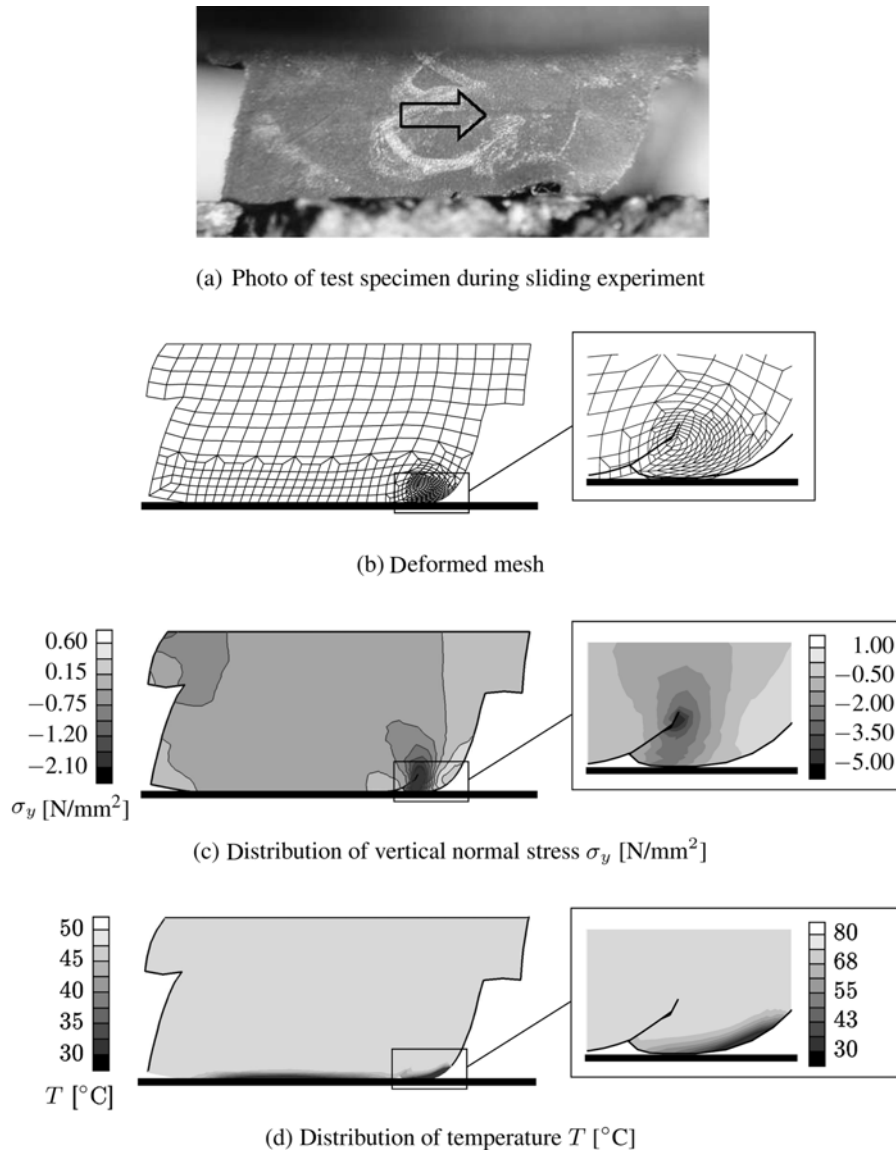


Fig. 8 State of rubber block at a sliding distance $g_T = 120$ mm for $p = 0.3$ N/mm² and $v = 300$ mm/s

the block tends to stick on the road surface. Consequently, the front edge curls up and causes a detachment of adjacent regions of the bottom surface of the rubber block from the road surface. A similar deformation behavior can be observed in experiments at the LFT (cf. Fig. 8a). High peaks of temperature and stresses at the front edge are the result of this behavior. The heating of the rubber block is limited to a thin layer adjacent to the contact interface, in which very steep temperature gradients occur. The reason for the strong limitation of the heated zone is the very low thermal conductivity of rubber and the short duration of a single run of the block in the simulation. Most of the rubber is unaffected by thermal processes. Therefore, it is admissible to consider the influence of the temperature on the behavior of the rubber block only by means of appropriate contact

formulations and to do the numerical simulations without temperature dependent material parameters.

5. Discussion and validation

The main items of the model for the numerical simulations are the material and the contact model. Their influence on the structural behavior of the considered rubber tread blocks is investigated in the next two subsections. Comparisons of the various formulations among each other are presented as well as comparisons with experimental results. The latter allow for validation of the different approaches and of the numerical simulation procedure in general.

5.1 Influence of material model

The influence of the material model on the simulation results is examined first. Numerical simulations using different formulations for the material behavior and various parameter sets are carried out for this purpose. The performance of the sliding rubber block is judged in relation to (i) its mechanical behavior (in terms of the stress field), (ii) its deformational behavior (in terms of the deformed contour), (iii) its thermal behavior (in terms of the temperature distribution at the surface),

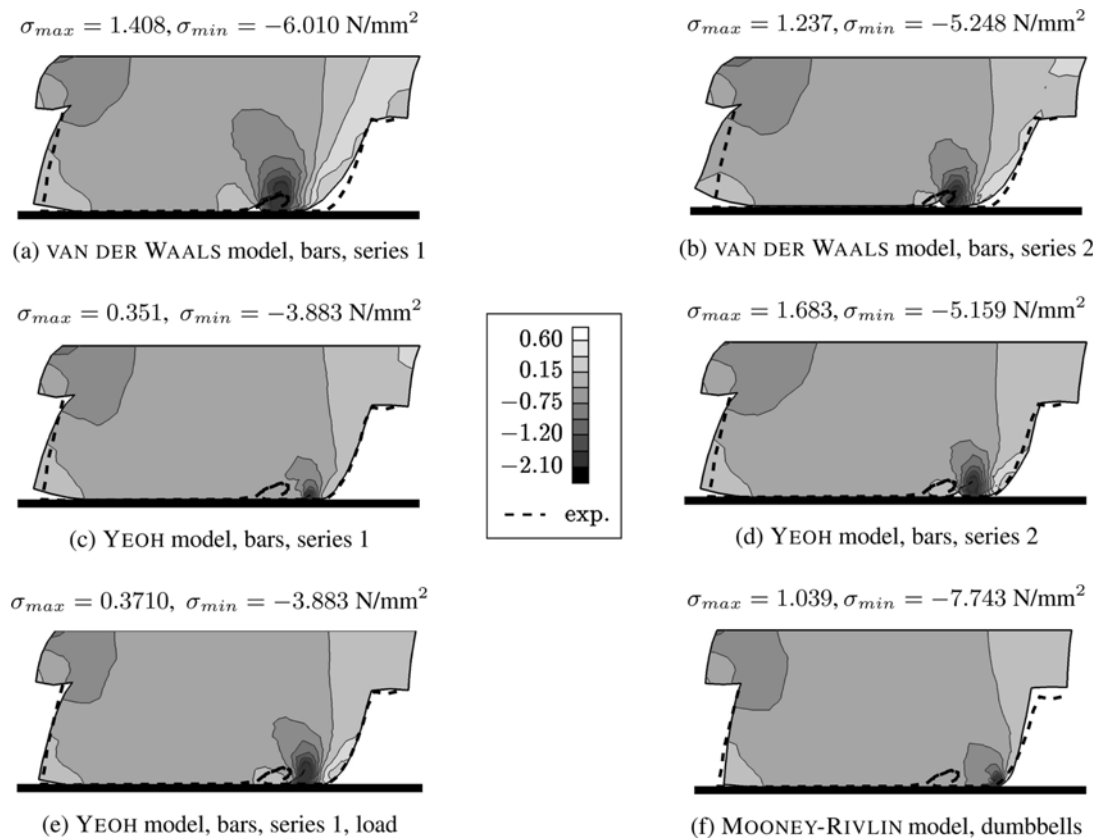


Fig. 9 Distribution of vertical normal stress σ_y [N/mm²] for different material models and parameter sets

and (iv) its frictional behavior (in terms of the resulting friction force). Experimental observations with respect to these quantities serve as the basis for validation.

Fig. 9 depicts the distributions of the stress component in vertical direction, σ_y , plotted on the deformed configuration of the block for different material descriptions. The results were obtained for average contact pressure $p = 3 \text{ N/mm}^2$, sliding velocity $v = 300 \text{ mm/s}$, and sliding distance $g_T = 120 \text{ mm}$. The maximum and minimum values of σ_y are specified in the headline of each plot.

The distributions of the stresses are rather similar in qualitative respects. The extreme values vary considerably, though no clear correlation exists between these values and the material stiffness deduced from the overall block deformation. In order to validate the deformational behavior, a block contour obtained from a photo of a block during tests at the LFT is included in all plots of Fig. 9. The application of the van der Waals formulation results in smaller deformations than use of the Yeoh model. This indicates a reduced material stiffness with the van der Waals model. Such a trend is encountered irrespective of the involved parameter sets (i.e., either “series 1” or “series 2” identified on basis of results from the first or second test series, respectively). For both formulations, larger deformations occur with the parameters from the second test series. The latter parameters represent a material behavior with a late upturn due to the high strain amplitude in the underlying experiments. Larger deformations in the simulations of the tread blocks are the natural consequence. The best agreement with the experimental contour is found for the Yeoh model under application of the parameter set with only loading data.

Fig. 10 shows the temperature distribution at the bottom surface of the rubber block for different material formulations. They correspond to the results depicted in Fig. 9 and, consequently, are based on the same settings of input parameters. The change of the material model does not affect this distribution considerably, since the friction parameters are the same irrespective of the involved material model. The only influence on the temperature curves results from variations of the deformational behavior of the rubber blocks under application of different material models. Expectedly, the deviations between the curves are not very pronounced, especially with regard to the maximum temperature in the interior of the bottom surface. The application of the Yeoh model with the parameter set based on only loading data yields the lowest peak value and, thus, comes closest to the experimental results. Surprisingly, the best overall match with the experimental curve is obtained for the Mooney-Rivlin model. Since the material model has only a minor effect on the friction temperatures, no superiority of the Mooney-Rivlin model can be deduced from this insight. The insufficient representation of the deformational behavior and the incapability of reproducing the

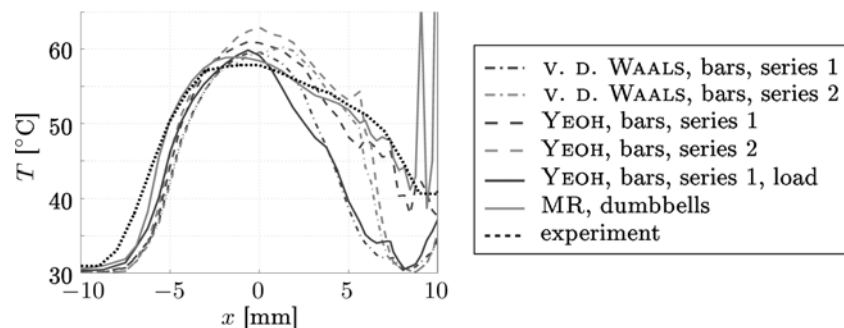


Fig. 10 Temperature distribution at the bottom surface of the rubber block for different material formulations and parameter sets

Table 4 Average values of the friction force $F_{T, \max}$ [kN] in the slip phase for different material formulations and parameter sets

van der Waals, bars, series 2	4.10	Yeoh, bars, series, 1	4.54
van der Waals, bars, series 1	4.56	Yeoh, bars, series, 1, load	4.86
Yeoh, bars, series 2	4.32	Mr, dumbbells	4.59

stiffening of the material at high strains are striking deficiencies of this model in the numerical simulations at hand.

Finally, the friction forces which build up during the sliding motion are examined in terms of average values of the friction force during the sliding phase. Table 4 provides a compilation of these forces for the different material models and parameters. As they reflect the friction conditions rather than the characteristics of the material, they are similar for all investigated material models.

5.2 Influence of the friction law

This subsection focuses on evaluating the two friction laws in view of their performance on a structural level. The term “performance” refers to the extent of agreement of simulation results with experimental observations for sliding blocks at the LFT. Main emphasis is placed on the evaluation of thermal results. These results are not employed in the identification of the parameters of the friction law. Thus, they emanate from independent measurements, though not from independent test series. The maximum temperature at the bottom surface of the rubber block and the integral over the temperature distribution at this surface are regarded as main characteristics. The maximum temperature refers to the peak value of the temperature distribution in the interior of this surface. Potential peak values at the front edge of the rubber block are not considered. These values are very much subject to inevitable changes of the test conditions between the experiments. Abrasion effects that are not considered in the presented default simulations have a strong influence on these peak values, too. The maximum temperature in the interior, T_{\max} , is not affected by the external conditions and by abrasion to such a high extent. Consequently, it is more suitable as comparative quantity in the evaluation procedure than the peak value at the edge. It characterizes the agreement of numerical and experimental results in quantitative respects.

The integral of the temperature increase over the bottom surface of the rubber block is denoted as A_T . It strongly depends on the shape of the temperature distribution at the bottom surface. Its evaluation gives evidence about the qualitative agreement of the temperature curves resulting from numerical simulations and experiments, respectively.

Prior to evaluation of T_{\max} and A_T , the temperature distribution at the bottom surface is examined in more detail. Fig. 11 shows this distribution for contact pressure $p = 0.3 \text{ N/mm}^2$ at three different sliding velocities. Numerical results obtained with the exponential relationship and the law by Huemer are depicted as well as experimental results from three test runs under equal conditions. All distinctive features of the temperature distribution can be studied on basis of these three examples. Variations of rubber compound or contact pressure do not change the course of the temperature distribution fundamentally.

Both friction laws result in very similar temperature distributions at all three velocities. The deviation of the curves referring to numerical and experimental results, respectively, is largest at $v = 7 \text{ mm/s}$ (cf. Fig. 11). The relative error computed as $\Delta T_{\max}/T_{\max, \text{exp}}$ is highest in this case. The

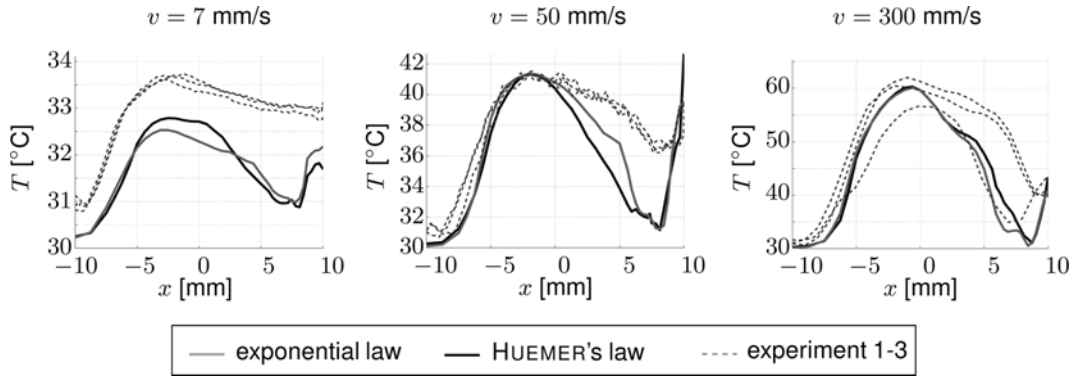


Fig. 11 Temperature distribution at the bottom surface of a rubber block at different sliding velocities – comparison of experimental and numerical results under application of the two friction laws

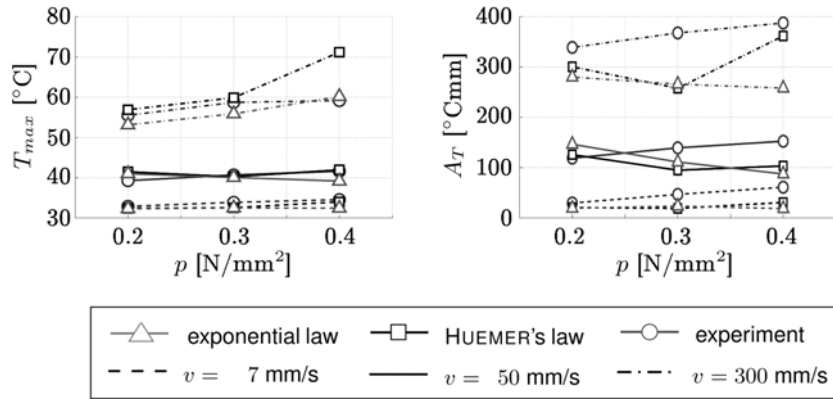


Fig. 12 Maximum temperature T_{max} at the bottom surface of the rubber block and area A_T under the temperature curve – comparison of experimental and numerical results under application of the two friction laws

absolute error ΔT_{max} , however, is comparable to the error obtained at $v = 50$ mm/s and $v = 300$ mm/s and, as regards T_{max} , rarely exceeds 1.5-2.0 °C. This appears to be sufficiently accurate. It does not make sense to claim for smaller differences, as the attainable accuracy of the experimental measurements is limited to 0.5-1.0 °C.

Fig. 12 shows a comparison of values for T_{max} and A_T obtained numerically with the exponential relationship or Huemer's law and experimentally, respectively. Results of all simulations, regarding tread blocks of different compounds, different contact pressures, and different sliding velocities, are included. The markers refer to discrete numerical and experimental results. The lines connecting these markers are intended to bring out the trends of the depicted quantities with increasing pressure.

The investigation of the plots in Fig. 12 demonstrates the very good agreement of numerical and experimental results under application of both friction laws. The differences between the results obtained with the two friction laws are surprisingly small. The general trends of the maximum temperatures depending on compound, velocity, and pressure are the same both times. At high velocities, the pressure dependence of the maximum value of temperature is more pronounced in the

simulations than in the experiments. This results in an overestimation of the temperatures at an average pressure $p = 0.4 \text{ N/mm}^2$ for all investigated combinations of the other input parameters. The overestimation is more pronounced for the friction law by Huemer than for the exponential one. At small velocities, the experiments yield almost no variation of T_{\max} with pressure. In the numerical simulations, a slightly decreasing trend of the temperatures is found at $v = 50 \text{ mm/s}$. This tendency is obtained with both friction laws. The differences between numerically and experimentally obtained values are more pronounced for A_T than for T_{\max} .

On the whole, also the simple exponential law gives a satisfactory performance. It must still be kept in mind that the exponential relationship fails to reproduce the experimentally observed peak of the friction coefficient at small sliding velocities. The material behavior of the considered compound exhibits a very low dependence on the excitation frequency and, thus, on the sliding velocity. The addressed incapacity of the exponential law does not affect its good performance in the numerical simulations for this reason. However, conditions change, when rubber compounds showing a frictional behavior with a pronounced velocity dependence are considered. The shortcoming of the exponential law is expected to be striking then.

6. Conclusions

This paper presents an efficient strategy for the simulation of rubber friction events in the framework of industrial applications. It provides thermo-mechanically coupled formulations for the contact behavior, which manage to combine the demands arising from industrial applicability on the one hand and the requirements of a high affinity to reality on the other hand. The use of a coupled approach allows for the simultaneous examination of stress and temperature fields in rubber blocks under consideration of their mutual interference. So far, most studies of rubber friction did concentrate on either the mechanical or the thermal problem. A profound investigation of frictional heating at the contact surface is not possible with this default separate treatment.

The application of the established numerical model was demonstrated considering the sliding of single rubber tread blocks on rough (road) surfaces as example. The simulation of such sliding processes is a common task in tire development. A purely macroscopic approach was chosen. This naturally sets boundaries to the capability of the simulations to map reality. However, the simulations themselves as well as the identification of involved model parameters are considerably simplified that ways.

Within the addressed limitations, the established procedure gives a very good performance. It is able to reproduce experimental results for a wide range of parameters as block geometry, rubber compound, contact pressure, or sliding velocity. Its suitability for the investigation of deformations (e.g., rolling of front edge), of thermal effects (e.g., temperature distribution at the bottom surface), and of the contact behavior (e.g., friction force) was demonstrated. The use of only readily-implemented options of the commercial FE code ABAQUS for the numerical simulations ensures its applicability for industrial use as, e.g., tire design and development.

The choice of a suitable material model is of decisive importance for a realistic deformational behavior of the rubber blocks in the simulations. The Mooney-Rivlin model, which does not capture the stiffening of the material at high strains, is not suitable in this respect. The material model affects not only the deformational behavior in the simulations, but also the numerical stability of the simulations. The application of an appropriate material model improves the performance of the

simulations, especially in regions of high local strains. The test data that is used for the identification of the material parameters has a very pronounced influence on the performance of the material model. It is essential to use data of a cycle, where the material behavior has already stabilized (i.e., where the influence of discontinuous damage is not pronounced any more) and of a sufficiently extensive strain range. An adjustment of strain ranges in experiments and the numerical simulations is mandatory.

The choice of the friction law within the framework of macroscopic formulations turned out to have no significant impact on the simulation results in terms of the thermal as well as the mechanical behavior of the rubber tread blocks.

The established simulation procedure naturally comprises some deficiencies. Currently a purely elastic material model is used. The use of a viscoelastic formulation for the material behavior regarding also effects of material damage would improve the reproduction of the real material behavior, especially in regions with high straining. At present, all investigated material formulations are more or less phenomenological[†]. The use of physically motivated formulations together with a suitable procedure for the identification of the involved parameters could additionally boost the affinity of the modeled material behavior to reality.

The contact model has a purely macroscopic foundation. The phenomenological characteristic of the involved parameters limits the predictive capabilities. The development of a suitable strategy on a microscopic basis for the derivation of formulations for the contact behavior would be preferable. This applies especially to the frictional heat generation, which is currently determined on basis of a comparison of experimental data and results of numerical resimulations at the structural level.

The addressed shortcomings of the current approach primarily arise from the focus of the established simulation procedure on industrializability and, thus, simplicity. The proposed improvements generally result in an increase of complexity of the numerical simulations and the involved formulations. Additional effort for model generation and parameter identification is the consequence. Whether the gain of quality and predictive capability at the expense of simplicity is favorable, must be judged in terms of the application at hand.

Acknowledgements

The presented work was part of a research project at the Continental AG.

References

- Chantrenne, P. and Raynaud, M. (2001), "Study of a macroscopic sliding contact thermal model from microscopic models", *Int. J. Thermal Sci.*, **40**, 603-621.
- Dorfmann, A. and Muhr, A. (1999), *Constitutive Models for Rubber*. Balkema: Rotterdam.
- Dorfmann, A. and Ogden, R.W. (2004), "A constitutive model for the Mullins effect with permanent set in particle-filled rubber", *Int. J. Solids Struct.*, **41**, 1855-1878.

[†]Also the van der Waals model is referred to as phenomenological in this context. Its parameters are determined in the default manner by fitting experimentally obtained stress-strain curves. This spoils the originally physical characteristic of the parameters of this model.

- Eberhardsteiner, J., Fidi, W. and Liederer, W. (1998), "Experimentelle Bestimmung der adhäsiven Reibeigenschaften von Gummiprüfungen auf ebenen Oberflächen (in German)", *Kautschuk Gummi Kunststoffe*, **51**(11), 773-781.
- Haraldsson, A. and Wriggers, P. (2000), "A strategy for numerical testing of frictional laws with application to contact between soil and concrete", *Comput. Meth. Appl. Mech. Eng.*, **190**, 963-977.
- Hofstetter, K. (2004), "Thermo-mechanical simulation of the sliding of rubber tread blocks", PhD-Thesis, Vienna University of Technology.
- Hofstetter, K., Grohs, Ch, Eberhardsteiner, J. and Mang, H.A. (2005), "Sliding behaviour of simplified tire tread patterns investigated by means of FEM", *Comput. Struct.*, accepted for publication.
- Huemer, T., Liu, W.N., Eberhardsteiner, J. and Mang, H.A. (2001), "A 3D finite element formulation describing the frictional behavior of rubber on ice and concrete surfaces", *Eng. Comput.*, **18**(3/4), 417-436.
- Kaliske, M. (1995), "Zur Theorie und Numerik von Polymerstrukturen unter statischen und dynamischen Einwirkungen (in German)", PhD-Thesis, Universität Hannover.
- Kaliske, M. and Rothert, H. (1997), "On the finite element implementation of rubber-like materials at finite strains", *Eng. Comput.*, **14**(2), 216-232.
- Klüppel, M. and Heinrich, G. (2000), "Rubber friction on self-affine road tracks", *Rubber Chemistry and Technology*, **73**(4), 578-605.
- Majumdar, A. and Tien, C.L. (1991), "Fractal network model for contact conductance", *J. Heat Transfer*, **113**, 516-525.
- Mikic, B.B. (1974), "Thermal contact conductance; theoretical considerations", *Int. J. of Heat and Mass Transfer*, **17**, 205-214.
- Ogden, R.W. (2001), "Pseudo-elasticity and stress softening", In *Nonlinear Elasticity: Theory and Applications*, Fu, Y.B., Ogden, R.W. (eds.). Cambridge University Press: Cambridge, 491-522.
- Persson, B.N.J. (2000), "Theory of rubber friction and contact mechanics", *J. Chem. Phys.*, **115**(8), 3840-3861.
- Sperling, L.H. (1992), *Introduction to the Physical Polymer Science* (2nd edn), John Wiley and Sons: New York.
- Twardzydło, W.W., Cecot, W., Oden, J.T. and Yew, C.H. (1998), "Computational micro- and macroscopic models of contact and friction: Formulation, approach and applications", *Wear*, **220**, 113-140.
- Williams, M.L., Landel, R.F. and Ferry, J.D. (1955), "The temperature dependence of relaxation mechanisms in amorphous polymers and other glass-forming liquids", *J. Am. Chem. Soc.*, **77**, 3701-3707.
- Wriggers, P. (2002), *Computational Contact Mechanics*, John Wiley and Sons, Chichester, England.